American Mineralogist, Volume 74, pages 432–438, 1989

Line-shape and thermal kinetics analysis of the Fe^{2+} band in Brazilian green beryl

SADAO ISOTANI, WAGNER W. FURTADO, RODOLFO ANTONINI, OSVALDO LUIS DIAS
Instituto de Física, Universidade de São Paulo, C.P. 20516, 01498 São Paulo, SP, Brazil

ABSTRACT

A study of optical-absorption spectra of the band of Fe^{2+} in the structural channels of isothermally treated beryl is reported. A linear correlation exists between the σ- and π-polarized components of the optical-absorption spectrum at around 12000 cm^{-1}. Irradiation with γ-rays from ^{60}Co causes a decrease of this band. The line-shape analysis shows two sites for Fe^{2+} at the structural channels. The kinetics analysis suggests a model in which Fe^{3+} is reduced to Fe^{2+} by release of holes from Fe^{3+} into the valence band. Subsequently, holes are retrapped by Fe^{2+} or annihilated by the recombination of electron and hole at a single deep trapping center. The untrapping parameter shows Arrhenius behavior. The retrapping and recombination parameters show a behavior proportional to $T^{1/2} - T_0^{1/2}$, which is explained with a free-electron distribution of hole velocities and a potential barrier of the trap.

INTRODUCTION

Beryl is a cyclosilicate with the chemical formula $Be_3Al_2Si_6O_{18}$ (Dana and Hurlbut, 1978). The crystal structure was determined by Bragg and West (1926). It belongs to the hexagonal system, and the unit cell contains two formula units. Beryl belongs to space group *P6/mcc*. The Si_6O_{18} rings form structural channels parallel to the unique crystallographic axis. The effective diameter of these structural channels varies from 2.8 Å in the plane of the Si_6O_{18} ring to 5.1 Å between two neighboring rings.

The blue color of natural beryl (aquamarine) is due to absorption bands in the near infrared. These bands have been attributed to Fe^{2+} impurity (Wood and Nassau, 1968; Samoilovich et al., 1971; Price et al., 1976; Parkin et al., 1977; Goldman et al., 1978; Blak et al., 1982). Several bands in the near infrared are known: the σ-polarized band at around 12000 cm^{-1} ($\mathbf{E} \perp \mathbf{c}$), π-polarized bands at around 10000 cm^{-1} and 12000 cm^{-1} ($\mathbf{E} \| \mathbf{c}$), and a band at around 16000 cm^{-1} in deep blue beryl.

The π-polarized bands were first attributed to Fe^{2+} in a channel site, and the σ-polarized band to Fe^{2+} in the sixfold-coordinated Al^{3+} site (Wood and Nassau, 1968; Samoilovich et al., 1971; Parkin et al., 1977). Price et al. (1978), on examining the Mössbauer and ESR spectra, concluded that the π-polarized bands arose from Fe^{2+} in the sixfold-coordinated site and suggested that the σ-polarized band arises from Fe^{2+} in the tetrahedral site. The deficiencies of some of these assignments were pointed out by Goldman et al. (1978): Fe^{2+} ion produces absorption bands in pairs because of the Jahn-Teller effect or geometric distortions of the coordination polyhedron; the molar absorbability is too high for the Al^{3+} site (Goldman and Rossman, 1977); and typical tetrahedral Fe–O bond distances are near 1.98 Å (Shannon and Prewitt, 1969), whereas Fe^{2+} must be accommodated into the 1.6-Å Be or Si site.

From structural similarities between cordierite and beryl, the optical-absorption study of cordierite (Goldman et al., 1977) was taken by us as the basis for the interpretation of the spectra of beryl. In the cordierite spectrum, Goldman et al. (1977) showed that two overlapping lines at 995 and 1170 mm arose from Fe^{2+} in the sixfold-coordinated site. Thus, the π-polarized bands of beryl arose from Fe^{2+} in the sixfold-coordinated Al^{3+} site, in agreement with Price et al. (1976), but the σ-polarized band arose from Fe^{2+} in the channels.

In beryl, the band at around 16000 cm^{-1} has been attributed to an Fe^{2+}-Fe^{3+} intervalence interaction (Samoilovich et al., 1971; Goldman et al., 1978).

The optical-absorption (OA) spectra of green and blue beryl from Minas Gerais, Brazil, reported by Blak et al. (1982), show only a single Fe band at around 12000 cm^{-1} ($\mathbf{k} \| \mathbf{c}$). Thus, in these samples, Fe^{2+} in the sixfold-coordinated site and Fe^{2+}-Fe^{3+} intervalence interaction are absent. It was suggested by Blak et al. that the single band asymmetry arose from the superposition of two bands.

The absence of Fe^{2+} in the sixfold-coordinated site and the Fe^{2+}-Fe^{3+} intervalence interaction give us a good chance to study the physical properties of Fe^{2+} in the beryl channels. Here, one purpose is the analysis of the asymmetry of the band at around 12000 cm^{-1} ($\mathbf{k} \| \mathbf{c}$) by the superposition of two bands, as proposed by Blak et al. (1982). Another purpose is the analysis of the thermal growth on heating, assuming a simplified microscopic model.

EXPERIMENTAL DETAILS

Samples of light green and colorless beryl, from Minas Gerais, Brazil, were kindly provided by A. R. Blak. The samples were cut in the form of parallelepipeds with two faces perpendicular and parallel to the **c** axis and about 5 mm thick.

0003–004X/89/0304–0432$02.00

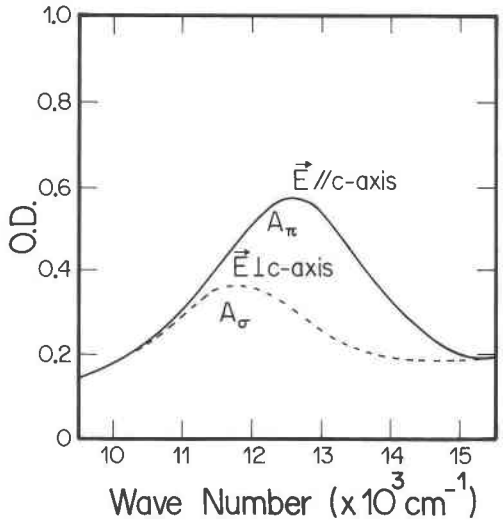

Fig. 1. Polarized spectra for $\mathbf{k} \perp \mathbf{c}$ axis of light green beryl.

A Carl Zeiss DMR21 spectrophotometer was used for the optical-absorption measurements. Polarized-light measurements were done with type II Polaroid.

The thermal treatments were done in air. The stability of the furnace with a useful volume of 10 × 12 × 15 cm was improved to 1 °C by filling with brick materials and two metallic plates. The temperature was measured using a chromel-alumel thermocouple, with one junction at 0 °C, an ECB X-T recorder, and a Keithley 160B digital multimeter. All the samples to be treated were put between previously heated metallic plates. With this arrangement, thermal equilibrium was achieved in the samples in about 40 s.

The samples were γ-irradiated using a ^{60}Co source (~400 000 Ci) from EMBRARAD S.A. at a rate of 80 × 10^3 Gy/h. The dose was controlled by means of three processes: ceric-cerous dosimetric system, AECL red acrylic dosimetric system, and UKAEA red perspex dosimeter.

Results

In Figure 1, we show the polarized spectra of the light green beryl for $\mathbf{k} \perp \mathbf{c}$ at around 12000 cm^{-1}. For $\mathbf{E} \perp \mathbf{c}$, the maxima are at 11700 cm^{-1}, and for $\mathbf{E} \| \mathbf{c}$, they are at 12750 cm^{-1}. For the sake of simplicity, we call the band at 11750 cm^{-1} ($\mathbf{E} \perp \mathbf{c}$) A_σ, and the band at 12750 cm^{-1} ($\mathbf{E} \| \mathbf{c}$) $\mathbf{A}_\pi$. The A_σ/A_π ratio of the maxima of the A_σ and A_π bands is about 0.5. The A_π band has not been previously reported, probably because it is masked by the superposition of the Fe^{2+} spectrum—also π-polarized—in the six-fold-coordinated Al^{3+} site.

The band position at around ~12000 cm^{-1} changes continuously from 11750 cm^{-1} (A_σ band, $\theta = 90°$) to 12750 cm^{-1} (A_π band, $\theta = 0°$), where θ is the angle between the electrical field direction $\mathbf{E}$ and the $\mathbf{c}$ axis. The band-position variation with θ is shown in Figure 2. The deformation in the 180° symmetry probably occurred because the sample was not cut with enough accuracy.

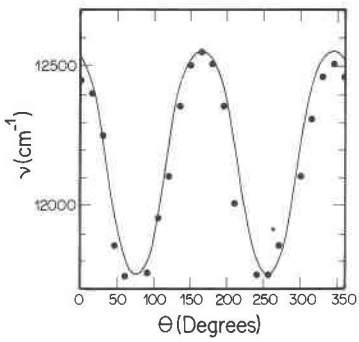

Fig. 2. Maxima of the ~12000 cm^{-1} band of light green beryl ($\mathbf{k} \perp \mathbf{c}$ axis) vs. the angle between $\mathbf{E}$ and $\mathbf{c}$ axis (● experimental; —— calculated).

In Figure 3, we show the correlation between the areas of the A_σ and A_π bands for the light green beryl treated isothermally at 411, 492, and 600 °C. The correlation is linear and about 0.5.

In Figure 4, we show the decrease of the unpolarized $\mathbf{k} \| \mathbf{c}$-axis band at around 12000 cm^{-1} for the colorless beryl irradiated with γ-rays. The decay curve is normalized to the band intensity of the nonirradiated sample.

Line-shape analysis

The A_σ and A_π bands have their band maxima close together. Thus, we propose that the band at around 12000 cm^{-1} observed for $\mathbf{k} \| \mathbf{c}$ by Blak et al. (1982) arises from the superposition of the A_σ and A_π bands.

To perform the proposed analysis, we need first to define the line shape of these bands. The breadth of a line may be due to several causes. The band is composed of

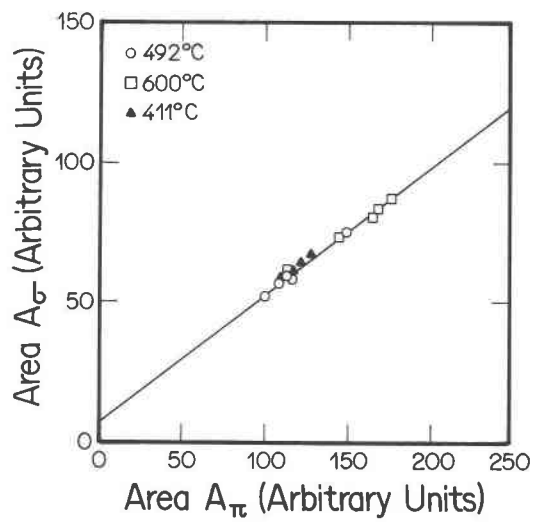

Fig. 3. Correlation between the areas of A_σ and A_π bands for isothermal treatments at 411, 492, and 600 °C of light green beryl.

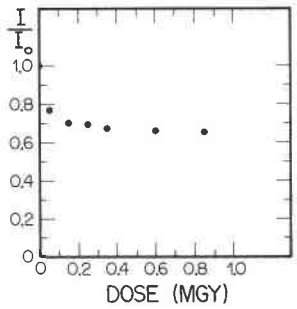

Fig. 4. Normalized intensity of the ~12000 cm^{-1} band (**k**∥**c** axis) vs. irradiation dose (γ rays from ^{60}Co) of colorless beryl.

narrow subbands, and the width arises from the uncertainty principle, from the interaction between centers, and from the dispersion of the normal modes. The envelope curve is due to the displacement of the normal modes during an optical transition. The overall shape can be approximated by several types of well-known line shapes: Gaussian, Lorentzian, double Gaussian, Pekarian, or the mixture of these lines. Markham (1959) has shown rigorously that for potential energies of ground and excited states with different minima, the shape gives a symmetrical curve at high temperature. Markham (1959) has shown that at room temperature, this condition is usually satisfied; thus a symmetrical line shape was assumed for modeling the room-temperature spectra. Also, from approximate evaluation, Markham (1959) has shown that the high-temperature absorption should be Gaussian. Thus a Gaussian line shape was assumed for modeling the room-temperature spectra.

Normalized A_σ and A_π line shapes were analyzed for natural light green beryl and for light green beryl heated to 600 °C. The relative wavenumber $\Delta\nu = \nu - \nu_0$, where ν is the wavenumber and ν_0 is the wavenumber at the maxima, is plotted in Figure 5. The line shape of the A_σ band showed only a small change on heating at 600 °C and had a width at half-height of about 960 cm^{-1}. Also, the line shape of the A_π band showed only a small change on heating at 600 °C and had a width at half-height of about 1200 cm^{-1}. The base line of the spectra introduces the largest portion of the uncertainty in the height of the bands for $|\Delta\nu| > 2000$ cm^{-1}, and error in the height measurement of the bands for $|\Delta\nu| < 2000$ cm^{-1} is estimated to be less than 5%.

A good fit was obtained for the Gaussian line shape by using the equations

$$A_\sigma = \exp\{-\ln 2[(\nu - 11750)^2/960^2]\}, \quad (1a)$$

and

$$A_\pi = \exp\{-\ln 2[(\nu - 12750)^2/1200^2]\}, \quad (1b)$$

where the data for the fit are normalized A_σ and A_π bands. The fit with these functions is shown in Figure 5.

We tested the above line shapes, analyzing the continuous variation of the band maximum ν_m at 12000 cm^{-1}

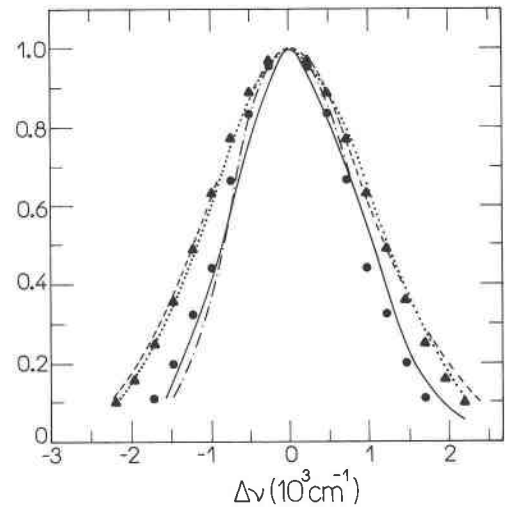

Fig. 5. Fit of the line shapes of the A_σ band (—— unheated; —·— heated at 600 °C; ● calculated) and A_π band (····· unheated; — — — heated at 600 °C; ▲ calculated).

(**k**⊥**c**) with the angle θ between **E** and the **c** axis. We assumed that the observed band is the superposition of A_σ and A_π lines. According to the Malus law (Strong, 1958), the band shape is written as

$$F(\nu) = A \sin^2\theta\, A_\sigma(\nu) + B \cos^2\theta\, A_\pi(\nu). \quad (2)$$

The band maximum ν_m was determined by equating to zero the first derivative of $F(\nu)$. Using the observed relation $A/B = A_\sigma/A_\pi \approx 0.5$, we obtained the equation

$$\sin^2\theta\,[(\nu_m - 11750)/960^2]f_\sigma + 2\cos^2\theta\,[(\nu_m - 12750)/1200^2]\,f_\pi = 0, \quad (3)$$

which was solved numerically for ν_m and θ. The result is shown as a solid line in Figure 2. The good agreement reinforces the use of the Gaussian line shape for the present analysis.

A good fit (Fig. 6) of the 12000 cm^{-1} band (**k**∥**c**) of green and blue beryl (Blak et al., 1982) was obtained using the equations

$$F_{green} = 0.526 + (12.3 \times 10^{-6})\nu + 0.176A_\sigma + 0.144A_\pi, \quad (4a)$$

$$F_{blue} = 0.238 + (46.9 \times 10^{-6})\nu + 0.148A_\sigma + 0.432A_\pi. \quad (4b)$$

From this fit, we concluded that the 12000 cm^{-1} (**k**∥**c**) band arises from the superposition of the A_σ and A_π bands.

The contribution of the A_σ and A_π bands in the green and blue beryl showed a ratio of about 1.22 and 0.34, respectively. The same relation, but for **k**⊥**c**, in light green beryl was 0.5. These observations suggested that the A_σ and A_π bands arise from two different Fe^{2+} centers in the structural channels of beryl.

The A_π band was not expected for the electric dipole transition in **k**∥**c** spectra, because **E** is in the plane perpendicular to the **c** axis, and so the condition **E**∥**c** is not

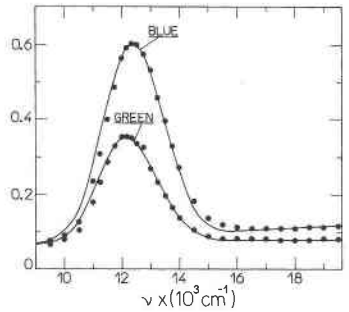

Fig. 6. Fit of the line shape of the ~12000 cm^{-1} band ($\mathbf{k}\|\mathbf{c}$ axis) in green and blue beryl (—— experimental; ● calculated).

allowed. However, the presence of the A_π band in the $\mathbf{k}\|\mathbf{c}$ spectra is allowed if we assume magnetic dipole transition. The magnetic field radiation, **B**, is perpendicular to the **c** axis for $\mathbf{k}\|\mathbf{c}$. Also, for the measurement of the A_π band ($\mathbf{k}\perp\mathbf{c}$), **B** is also perpendicular to the **c** axis. Usually the magnetic dipole process is a weaker process, since the maximum possible values of the matrix elements $\langle f|\, Y\boldsymbol{\mu}\cdot\mathbf{B}\,|i\rangle$ (i, f = initial and final states, $Y\boldsymbol{\mu}$ = magnetic dipole operator) are smaller than the possible values of the matrix elements of $\langle f|\, P\mathbf{p}\cdot\mathbf{E}\,|i\rangle$ ($P\mathbf{p}$ = electric dipole moment operator) (Imbusch, 1978, p. 23). However, when a radiative transition is forbidden for an electric dipole process, a magnetic dipole process may occur. In the present case, for $\mathbf{k}\|\mathbf{c}$, the electric dipole process is forbidden for A_π because **E** will be never parallel to the **c** axis. Thus, the A_π band is allowed for $\mathbf{k}\|\mathbf{c}$ by the magnetic dipole process.

Kinetics

The isothermal decay kinetics of the reduction of Fe^{3+} to Fe^{2+} was determined by Blak et al. (1982) for green beryl from Minas Gerais, Brazil. An empirical analysis of the decay kinetics of the EPR of the Fe^{3+} line using a sum of two first-order processes (Levy et al., 1974) showed activation energies 0.30 and 0.46 ev. Also, it was shown that at room temperature, the expected half-life of Fe^{3+} from this analysis was 7.5 and 1.5 hr, respectively. These results indicate that no green beryl should be found in nature. Since this is not true, it was concluded that there is a minimum temperature necessary for the reduction of Fe^{3+} to Fe^{2+}. Thus, by measuring $I(t_{1/2})/I(t=0)$ at several temperatures below 400 °C, it was shown that the Fe^{3+} reduction to Fe^{2+} stops at about 200 °C.

As the empirical model does not explain why the reduction stops at 200 °C, we examined the Blak et al. (1982) data according to the microscopic method for the analysis of kinetics (see Curie, 1963, p. 150). The previous analysis of Blak et al. using the sum of two first-order kinetics allows the comparison of the two methods.

Here we assumed a model where Fe^{3+} is reduced to Fe^{2+}, through the thermally induced release of holes from Fe^{3+} ions into the valence band. Also, we assumed that these valence holes recombine with electrons trapped at a single deep trapping center. In Figure 7, we show a sketch of the process proposed here.

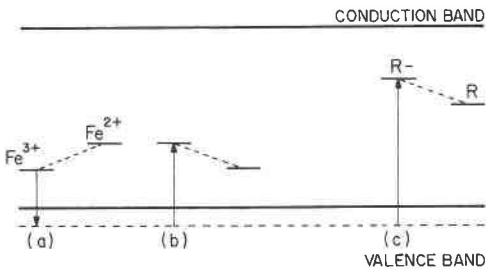

Fig. 7. Sketch of the kinetic process.

Process *a* is the result of the thermal reduction of Fe^{3+} to Fe^{2+} through the release of a hole into the valence band. Process *b* is the capture process (oxidation) of a valence hole by Fe^{2+}, thus giving Fe^{3+}, a process that we call retrapping of a hole. Process *c* is the electron-hole annihilation in the R center, which we call recombination of a hole. The R center is a center produced by the capture of an electron in a crystal defect, giving a deep level. The kinetic equations for this model are (Curie, 1963, p. 174)

$$\frac{d}{dt}[Fe^{2+}] = \alpha/\{[Fe]_0 - [Fe^{2+}]\} - \gamma[Fe^{2+}][h^+], \tag{5a}$$

and

$$\frac{d}{dt}[h^+] = \frac{d}{dt}[Fe^{2+}] - \beta\{[Fe] - [Fe^{2+}] + [h^+]\}/[h^+], \tag{5b}$$

where $[Fe^{2+}]$, $[h^+]$, and $[Fe]_0$ are the concentrations of Fe^{2+}, holes, and iron ($[Fe^{3+}] + [Fe^{2+}]$).

We evaluated these equations for $[Fe^{2+}]$ using the method of Runge-Kutta (Milne, 1970). The normalization of the above equations was done on the initial concentration of Fe^{2+}, giving the conditions $[Fe^{2+}](0) = 1$ and $[h^+](0) = 0$.

Figure 8 shows the growth curves of the A_σ band for isothermal treatments at 400, 450, 490, 550, and 600 °C from Blak et al. (1982). The growth curves in Blak et al. were given as $(I/I_0) - 1$ vs. dose, where I is the optical-

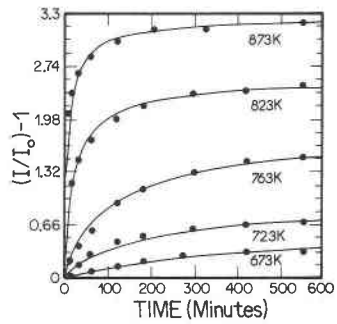

Fig. 8. Normalized growth curves of A_σ band for isothermal treatments at 400, 450, 490, 550, and 600 °C (● experimental; —— calculated) of green beryl.

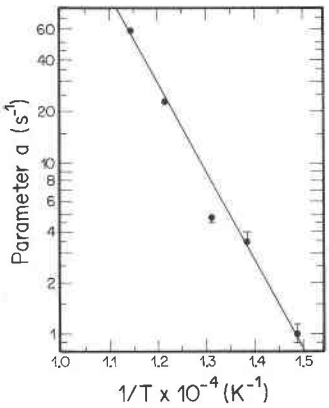

Fig. 9. Parameter α vs. VT showing Arrhenius law.

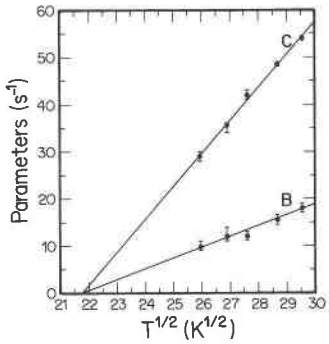

Fig. 10. Parameters B and C vs. $1/T$ showing linear correlation with $(T^{1/2} - T_0^{1/2})$.

absorption intensity of heated green beryl and I_0 is the optical-absorption intensity of unheated green beryl. The definition $(I/I_0) - 1$ is the relative actual concentration of Fe^{2+}. Thus, we have $[Fe^{2+}] = (I/I_0) - 1$.

The fit of the calculated $[Fe^{2+}]$ with the experimental data was obtained using the trial and error method. The best-fit parameters are shown in Table 1.

The parameter α follows the Arrhenius law as shown in Figure 9. The fit gives an activation energy ΔE of 1.03 ev, and the frequency factor is $4.74 \times 10^7\ s^{-1}$.

The activation energy determined above is about twice the activation energies obtained by Blak et al. (1982): 0.46 ev and 0.3 ev. We attribute this difference to the retrapping process that slows the kinetics, increasing the activation energy in the fit.

The parameters $C = \gamma/[Fe^{2+}](0)$ and $B = \beta/[Fe^{2+}](0)$ show a linear correlation with $T^{1/2}$ (Fig. 10). This correlation with $T^{1/2}$ also shows that there is a temperature $T_0 \approx 473$ K where these parameters become zero. This means that the kinetic process, which concerns retrapping and R electron-hole recombination, ceases.

The present analysis of the behavior of parameters B and C with temperature agrees well with the observation that Fe^{3+} reduction to Fe^{2+} stops at about 200 °C (Blak et al., 1982).

Interpretation of the kinetics parameters

The $T^{1/2}$ behavior is the result of the free-particles approximation, as we will show. Let us consider N conduction holes that, through collisions with another N' removing centers, remove one hole per collision from the set N. Thus, the change in N, dN, when the holes travel a distance dx is given by (Sears, 1963, p. 259)

$$dN = -PN\,dx, \tag{6}$$

where P is the collision probability, which is given by the product of the hole-center collision cross section, σ, with the number of centers, N'. Assuming that the holes travel with speed v in a time interval dt, we obtain the rate equation

$$dN/dt = -PNv. \tag{7}$$

The N holes have different speeds. The rate equation for ΔN_i holes with speed v_i is

$$d\Delta N_i/dt = P\,\Delta N_i v_i. \tag{8}$$

The sum of speeds over all possible groups gives the rate equation for N:

$$dN/dt = -\sum P\,\Delta N_i v_i. \tag{9}$$

Table 1. Parameters fit for the kinetic Equations 5a and 5b for Fe^{2+} OA band in Brazilian green beryl

T (K)	α		γ		β		N	
673	1.00	+0.15 −0.10	29	+1 −1	9.8	+1.2 −0.8	1.90	+0.01 −0.01
723	3.5	+0.5 −0.1	35.6	+0.4 −1.6	12	+2 −1	2.00	+0.01 −0.01
763	4.8	+0.1 −0.3	42	+1 −1	12	+1 −1	2.90	+0.01 −0.01
823	23	+1 −1	48.5	+0.5 −0.5	15.5	+1 −1	3.50	+0.01 −0.01
873	59	+1 −1	54.0	+0.5 −0.5	18	+1 −1	4.23	+0.01 −0.01

Then for $\Delta N_t \to 0$, we obtain

$$dN/dt = -\int_{\text{all}} Pv\, dN. \quad (10)$$

We assume that the holes in the valence band behave roughly as free particles. Thus we write for dN the free-particles distribution (Sears, 1963, p. 235):

$$dN = (4N/\sqrt{\pi})\,[(m/2kT)]^{3/2}v^2\exp[-(mv^2/2kT)]\,dv. \quad (11)$$

Evaluating the rate equation for this distribution and using the definition of P, we obtain

$$dN/dt = -\sigma\bar{v}NN', \quad (12)$$

where

$$\bar{v} = \sqrt{8kT/\pi m}.$$

The existence of T_0 is probably a consequence of different local distortions produced by Fe^{2+} and Fe^{3+}. The change of the local distortion from Fe^{3+} to Fe^{2+} requires energy, giving rise to a potential barrier.

Holes that are released from the trapping centers with smaller energy than the potential barrier, are released by a tunneling process, giving small concentrations. Thus, the kinetics of these holes make a small contribution to the kinetics.

The holes thermally released will have an energy K_0. This energy gives rise to a minimum speed $v_0 = \sqrt{2K_0/m}$ for the holes. This implies that there will not be holes with $v < v_0$, changing the distribution of holes used here. We assume that the limit of speed is satisfied for

$$dN/dt = -\sigma(\bar{v} - v_0)NN'. \quad (13)$$

Assuming $v_0 = \sqrt{8kT_0/\pi m}$ we obtain

$$dN/dt = -\sigma\sqrt{(8k)/(\pi m)}(\sqrt{T} - \sqrt{T_0})NN'. \quad (14)$$

This temperature dependence was found here for B and C, giving good support for the present assumptions.

Discussion

Irradiation of colorless beryl from Minas Gerais, Brazil, showed the oxidation of Fe^{2+} to Fe^{3+}. On the other hand, Blak et al. (1982) through OA and EPR studies of beryl showed that Fe^{3+} in Al^{3+} substitutional sites in blue beryl is not reduced on heating, whereas Fe^{3+} in green beryl in the channels is reduced, showing that the reduction process occurs only for Fe^{3+} in the structural channels.

From line-shape analysis we showed that the band at around 12000 cm^{-1} is the superposition of two σ- and π-polarized bands (A_σ and A_π bands, respectively). The different contributions of the A_σ and A_π bands to the line shapes of light blue, blue, and green beryl show that these bands are due to Fe^{2+} at two different sites in the structural channels. This observation is apparently contradictory with the similar kinetics obtained for the A_σ and A_π bands, as shown in Figure 8.

It was shown by Wood and Nassau (1968) that water molecules in beryl occupy two sites in structural channels: site I (type I) with the water's C_2 symmetry axis perpendicular to the crystal **c** axis and site II (type II) with the water's C_2 symmetry axis parallel to the crystal **c** axis. The type I water molecule is predominant in blue beryl, whereas the type II water molecule is predominant in green beryl (Blak et al., 1982).

Ions of Fe can be found in the structural channels without a neighbor water molecule or with a neighbor type II water molecule. A neighbor type I water molecule is less probable because water's polarity gives a lower-energy configuration if the Fe-O axis lies along the water's C_2 axis. The crystal-field symmetry of a water-free Fe^{2+} will be different from that of a water-associated Fe ion. Thus we suggest that the A_σ band is due to water-free Fe^{2+} and the A_π band to Fe^{2+}-associated with type II water.

In blue beryl, the alkali content is small as shown by the predominant type I water molecule IR bands (Blak et al., 1982). This supports the association of Fe^{2+} with water. Otherwise, in green beryl, the alkali content is high, as shown by the predominant type II water molecule IR bands. This does not support the association of Fe^{2+} with water. Thus the A_π band is expected to be bigger in blue beryl. This agrees with the observed relation $A_\sigma/A_\pi = 1.22$ in green beryl and $A_\sigma/A_\pi = 0.34$ in blue beryl.

A good fit resulted from the analysis of the kinetics with the model where Fe^{2+} oxidation occurs through hole untrapping to the valence band, hole retrapping by Fe^{3+}, and recombination of holes with electron centers. The parameters related to the retrapping and electron-hole recombination showed a $T^{1/2}$ behavior derived from free-particle approximation and a cut-off temperature T_0 that agrees well with cessation of the reaction at around 200 °C (Blak et al., 1982). The electron density of the valence band is essentially around lattice ions, i.e., around Be^{2+}, Al^{3+}, Si^{4+}, and O^{2-} ions. The channel's Fe^{3+} nearest-lattice ions are O^{2-}. Thus, the hole untrapping must occur through the $Fe^{3+} + O^{2-} \to Fe^{2+} + O^-$ reaction and then through $O^- + O^{2-} \to O^{2-} + O^-$ chain migration through the valence band. The neighbor water molecule does not affect the untrapping nor the retrapping parameters because it does not take part in the crystal structure. This observation makes consistent the observation of different optical-absorption spectra with similar kinetic parameters of the two channel Fe^{2+} ions (with and without a neighbor water molecule).

Acknowledgments

We would like to thank Professor Clemencio Teodoro Dotto for his collaboration in the computation part of this work. This work was partly supported by grants from CAPES-PICD, CNPq, FINEP, and FAPESP.

References cited

Blak, A.R., Isotani, S., and Watanabe, S. (1982) Optical absorption and electron spin resonance in blue and natural beryl. Physics and Chemistry of Minerals, 8, 161–166.

Bragg, W.L., and West, J. (1926) The structure of beryl $Be_3Al_2Si_6O_{18}$. Proceedings of the Royal Society of London, ser. A, 111, 691–714.

Curie, D. (1963) Luminescence in crystals. Methuen, London.

Dana, J.M., and Hurlbut, C.S., Jr. (1978) Dana's manual of mineralogy. Livros Técnicos e Científicos, Rio de Janeiro.

Goldman, D.S., and Rossman, G.R. (1977) The identification of Fe^{2+} in the M(4) site of calcic amphiboles. American Mineralogist, 62, 205–216.

Goldman, D.S., Rossman, G.R., and Dollase, W.A. (1977) Channel constituents in cordierite. American Mineralogist, 62, 1144–1157.

Goldman, D.S., Rossman, G.R., and Parkins, K.M. (1978) Channel constituents in beryl. Physics and Chemistry of Minerals, 3, 225–235.

Imbusch, G.F. (1978) Inorganic luminescence. In M.D. Lumb, Ed., Luminescence spectroscopy. Academic Press, London.

Levy, P.W., Mattern, P.L., Lengweiler, K., and Bishay, A.M. (1974) Studies on non metals during irradiation: V. Growth and decay of color centers in barium aluminoborate glass containing cerium. Journal of the American Ceramic Society, 57, 176–181.

Markham, J.J. (1959) Interaction of normal modes with electron traps. Reviews of Modern Physics, 31, 956–989.

Milne, W.F. (1970) Numerical solution of differential equations. Dover Publications, New York.

Parkin, K.M., Loefler, B.M., and Burns, R.G. (1977) Mössbauer spectra of kyanite, aquamarine, and cordierite showing intervalence charge transfer. Physics and Chemistry of Minerals, 1, 301–311.

Price, D.C., Vance, E.R., Smith, G., Edgar, A., and Dickson, B.L. (1976) Mössbauer effect studies of beryl. Journal de Physique, 37, Colloque C, Supplement 12, 147–150.

Samoilovich, M.I., Tsinober, L.I., and Dunin-Barkoviskii, K.L. (1971) Nature of coloring in iron-containing beryl. Soviet Physics–Crystallography, 16, 147–150.

Sears, F. W. (1963) Thermodynamics, the kinetic theory of gases and statistical mechanics. Addison-Wesley, Reading, Massachusetts.

Shannon, R.D., and Prewitt, C.T. (1969) Effective ionic radii in oxides and fluorides. Acta Crystallographica, B25, 925–946.

Strong, J.W.H. (1958) Concepts of classics optics. Freeman, San Francisco.

Wood, D.L., and Nassau, K. (1968) The characterization of beryl and emerald by visible and infrared absorption spectroscopy. American Mineralogist, 53, 777–800.

Manuscript received March 21, 1988
Manuscript accepted October 31, 1988